

the highest concentrations of dissolved solids.

The high calcium concentrations are a major factor in the continuous formation of phosphate-bearing minerals such as hydroxylapatite [$\text{Ca}_5(\text{PO}_4)_3\text{OH}$] and fluorapatite [$\text{Ca}_{10}(\text{PO}_4)_6\text{F}_2$] throughout the lake. In addition, the lake is oversaturated with calcite (CaCO_3) throughout the year except during the middle and late winter when the pH falls below 7.

Since Onondaga Lake serves as a receptacle for an area that is almost entirely urban, there is little contribution of phosphorus from natural and agricultural sources. Preliminary estimates of the influent total inorganic phosphorus indicate that approximately 71 percent can be accounted for by municipal point-source discharges, 19 percent by municipal nonpoint sources (combined sewer overflows), 1 to 2 percent by industrial sources, and 8 to 9 percent by agricultural and natural sources (8). Natural sources have been reported to account for 26 to 41 percent of the phosphorus discharged to the receiving water bodies in the continental United States. It has been predicted that elimination of phosphates from detergents might result in the reduction of the average total phosphorus concentrations in receiving waters from 0.26 to 0.18 mg/liter for a reduction of 37.7 percent (9). The legislation limiting phosphates in detergents has had a much more pronounced effect on Onondaga Lake, reducing the

average concentration of total inorganic phosphorus from 1.74 to 0.74 mg/liter—a net change of 57.4 percent.

It is evident that the limitation of detergent phosphate composition to 8.7 percent phosphorus by weight has had a discernible effect on the chemical and biological composition of the lake. Perhaps, therefore, a harder look should be given to the use of this type of legislation by State and Federal regulatory agencies in the control of cultural eutrophication. Due to present domestic fiscal policy limitations, legislation of this nature may be one of the effective methods of controlling eutrophication in the immediate future.

C. B. MURPHY, JR.
O'Brien & Gere Engineers, Inc.,
1304 Buckley Road,
Syracuse, New York 13201

References and Notes

1. R. D. Grundy, *Environ. Sci. Technol.* **5**, 1184 (1971).
2. New York State Legislature, Laws of 1971, chap. 716.
3. The monitoring program was conducted jointly by Onondaga County Department of Public Works and O'Brien & Gere Engineers, Inc., Syracuse, New York.
4. *Standard Methods for the Examination of Water and Waste Water* (American Public Health Association, New York, ed. 12, 1965), pp. 234-237.
5. J. Shapiro, *Science* **179**, 382 (1973).
6. R. Margalef, *Perspectives in Ecological Theory* (Univ. of Chicago Press, Chicago, 1968), p. 111.
7. "Onondaga Lake study," report to the Water Quality Office of the Environmental Protection Agency, on EPA Project 11060 FAE (April 1971).
8. C. B. Murphy, unpublished results.
9. F. A. Ferguson, *Environ. Sci. Technol.* **2**, 188 (1968).

23 March 1973; revised 18 June 1973 ■

Mars: Mariner 9 Spectroscopic Evidence for H₂O Ice Clouds

Abstract. *Spectral features observed with the Mariner 9 interferometer spectrometer are identified as those of H₂O ice. The measured spectra are compared with theoretical calculations for the transfer of radiation through clouds of ice particles with variations in size distribution and integrated cloud mass. Comparisons with an observed spectrum from the Tharsis Ridge region indicate H₂O ice clouds composed of particles with a mean radius of 2.0 micrometers and an integrated cloud mass of 5×10^{-5} gram per square centimeter.*

Ground-based observations indicate that several distinct types of clouds occur in the martian atmosphere including yellow clouds, assumed to be composed of blowing surface dust, and white clouds, assumed to be condensed volatile substances (1). White clouds fall into two classes: (i) diffuse clouds with no particular aerographic location and (ii) discrete clouds at relatively fixed aerographic locations (2). Discrete clouds have been observed in the

Nix Olympica-Tharsis Ridge area by Slipher (3), in the near-encounter pictures of Mariner 7 (4), and in the Mariner 9 orbital pictures (5). Although it has been suspected that the white clouds are composed of H₂O ice (6), to date no direct spectral evidence has been found. We present here spectroscopic data indicating the existence of H₂O ice clouds on Mars in the region of the shield volcanoes of the Tharsis Ridge. Estimates are given for

the cloud particle size and the integrated cloud mass.

Spectra of Mars have been obtained between 200 and 2000 cm^{-1} with a resolution of 2.4 cm^{-1} by the infrared interferometer spectrometer (IRIS) carried by the Mariner 9 spacecraft. The observed spectral interval includes the molecular absorption features of both CO₂ and H₂O. Observations of these spectral features and their use in determining surface pressure, thermal structure, and the amount of H₂O vapor have appeared in the literature (7). Broad absorption features, indicative of particulate (dust) absorption, have also been observed during the Mariner 9 mission. Spectra obtained in the later part of the mission show additional broad absorption features which differ in position and width from those of the dust clouds. These broad absorption features were found to correspond closely to those expected for H₂O ice clouds.

Figure 1A presents a comparison of spectra observed in the Tharsis Ridge region and the lower Arcadia region with theoretical calculations for an H₂O ice cloud. The spectrum measured over lower Arcadia shows an approximately constant brightness temperature except for the CO₂ absorption band centered at 667 cm^{-1} and the rotational H₂O vapor absorption lines below 400 cm^{-1} . In contrast, the Tharsis Ridge spectrum exhibits a strikingly broad absorption feature extending from 550 to 950 cm^{-1} with a second broad absorption region evident between 225 and 350 cm^{-1} . Superimposed on the latter is a sharp spectral feature near 227 cm^{-1} . The theoretical H₂O ice cloud spectrum (Fig. 1B), described below, exhibits a similar behavior.

The IRIS fields of view for the two observed spectra are indicated in Fig. 2 by circles superimposed on a Mariner 9 television picture of the same region. Prominent in the picture are the summits of Nix Olympica and of the three shield volcanoes along the Tharsis Ridge as well as the extensive cloud systems to the west of the volcanoes. Because of the substantial processing of the television data, information concerning the optical properties of the clouds cannot be inferred visually from Fig. 2. The cloud-free spectrum is associated with the field of view in the left portion of Fig. 2, whereas the ice cloud spectrum from the field of view in the center of the figure includes the clouds off North Spot and Middle Spot. Since

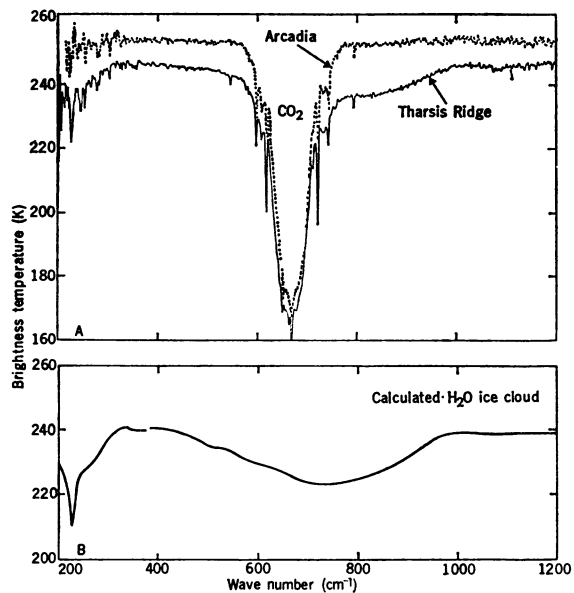


Fig. 1. (A) Mariner 9 IRIS measurements of the lower Arcadia region under clear conditions and of the Tharsis Ridge region under conditions of partial cloudiness. The Arcadia spectrum is displayed vertically for clarity. The Tharsis Ridge spectrum shows broad absorption features from 550 to 950 cm^{-1} and from 225 to 350 cm^{-1} , similar to those of the theoretical H_2O ice cloud spectrum shown in (B).

the summits of the volcanoes are visible in Fig. 2, the bulk of the associated clouds must be near or slightly below these summits.

The theoretical calculations are based on the theory of radiative transfer in a scattering atmosphere containing spherical particles with the refractive index of H_2O ice. The transfer calculations include a numerical integration

of the solution to the equation of radiative transfer over discrete atmospheric layers and over an angular mesh. The numerical integration is similar to that used by Herman and Browning (8) for visible wavelengths. The complex refractive indices of H_2O ice were used to calculate the absorption and scattering cross sections per unit volume and the angularly dependent phase matrix

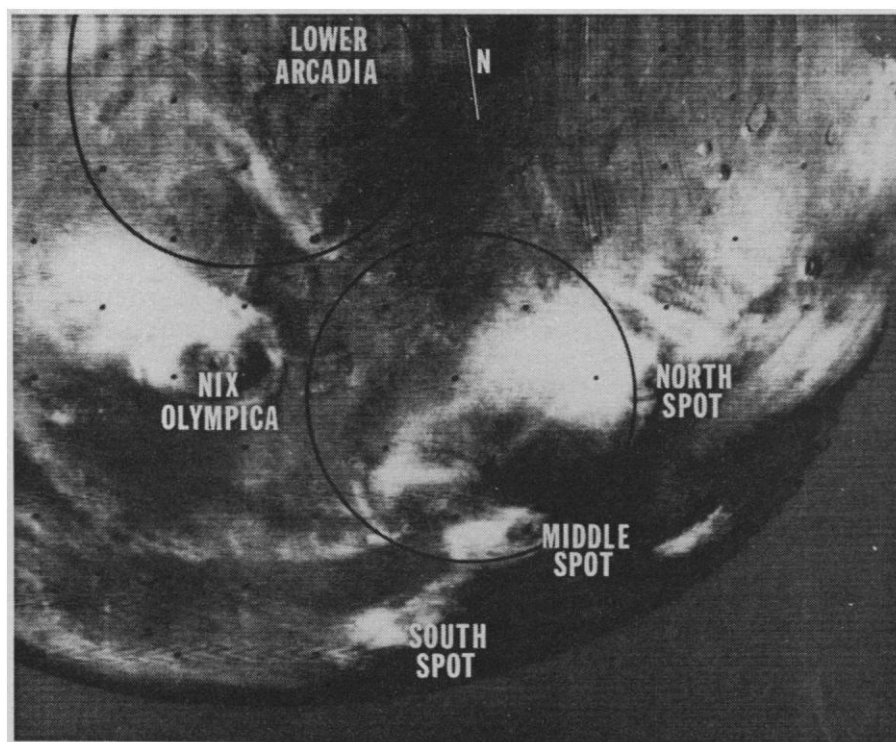


Fig. 2. The IRIS fields of view superimposed on a television photograph taken at nearly the same time as the spectral measurements. Indicated on the photograph are the summits of Nix Olympica and of the three shield volcanoes along the Tharsis Ridge—North Spot, Middle Spot, and South Spot.

for a distribution of particle sizes. The assumed spherical shape appears to be a reasonable first approximation even for nonspherical particles when the wavelength of the radiation is much larger than the particle dimensions. This was found to be the case for the wavelengths and particle sizes encountered in this study. The size distribution used for the calculations presented in Fig. 1 had a mean particle radius of 4.6 μm and a mode radius of 4.0 μm , and fell to one-tenth of its maximum value at 2.3 and 5.7 μm . Ice refractive indices for wave numbers less than 380 cm^{-1} were obtained from Bertie *et al.* (9), and those for wave numbers greater than 380 cm^{-1} were obtained from recent measurements of Schaaf and Williams (10). The laboratory measurements of Bertie *et al.* were carried out using ice cooled to 77 K and the measurements of Schaaf and Williams using ice cooled to 268 K. The latter temperature more closely approximates martian conditions. The use of two different sources for the refractive indices causes a small discontinuity in the calculated spectrum at 380 cm^{-1} . The cloud temperature was chosen from the atmospheric temperature distribution derived from the spectrum for the clear region; because the two spectra were obtained from the same general geographic area and at nearly the same time, it was assumed that the temperature profile from the clear spectrum was also applicable for the Tharsis Ridge spectrum. The summits of the great shield volcanoes extend very high into the atmosphere (11) and are generally situated between the 0.5- and the 1.0-mbar pressure levels. Temperatures corresponding to these altitudes in the lower Arcadia region are 170 to 180 K. The top of the ice cloud was assumed to be slightly below the summit altitude at a temperature of 180 K and with a constant particle number density in a layer 1 km thick. In addition to being sensitive to the cloud top temperature, the calculated spectra are dependent on the integrated cloud mass per unit area, which may be related to the visible optical thickness of the cloud, and on the mean radius of the particles. The results of theoretical calculations in the spectral interval from 50 to 2000 cm^{-1} for ice clouds of different visible optical thicknesses are shown in Fig. 3A with the cloud particle size distribution having a mean value equal to 4.6 μm . The cor-

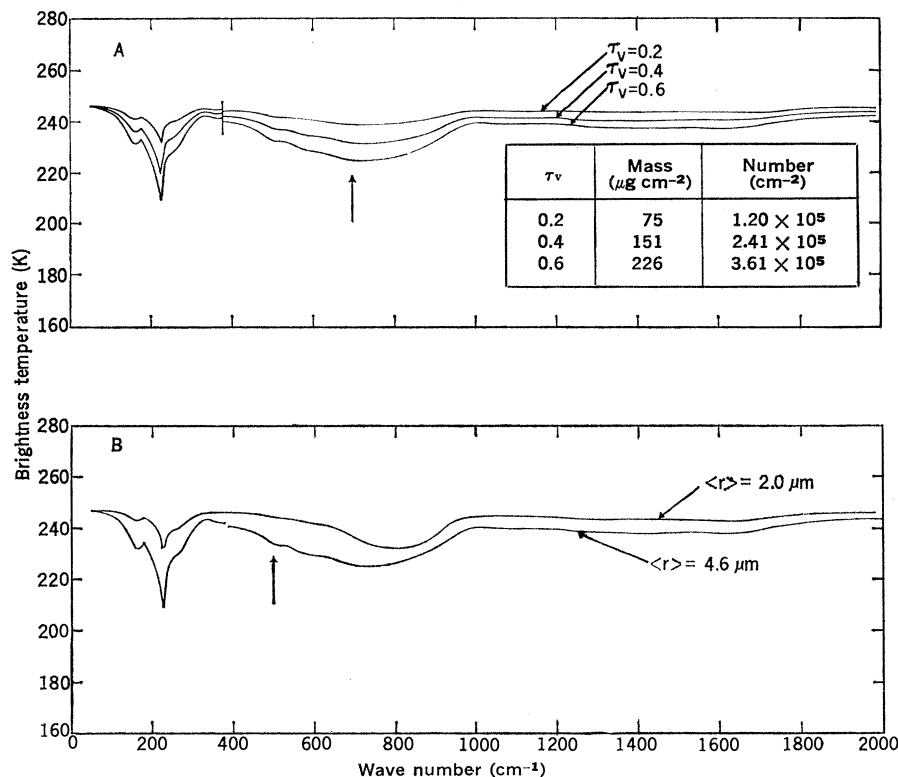


Fig. 3. Results of calculations made for variations in cloud visible optical thickness τ_v (A) and in particle size distribution (B). The arrows indicate the position of greatest independent variation in brightness temperature with respect to each variable.

responding integrated cloud mass per unit area and the number of particles per unit area are shown in the inset. For each calculated spectrum the total number of particles in the cloud was adjusted to give the visible optical depth indicated. Increasing the visible optical depth was found to strengthen the infrared attenuation throughout the spectrum and to preferentially strengthen the absorption features near 227 and 750 cm^{-1} . Variation of the cloud top temperature produced an effect similar to a variation of the visible optical thickness of the cloud. Therefore, it is not possible to uniquely determine both a cloud top temperature and the visible optical thickness from the infrared spectral measurements alone.

The dependence of the emergent spectrum on the size distribution of the cloud particles may be characterized by a mean particle radius $\langle r \rangle$. Figure 3B shows spectra calculated for two different particle size distributions, assumed to be the modified gamma-distributions as discussed by Deirmendjian (12). The major effect of variation of the particle size distribution occurs near 500 cm^{-1} where the refractive indices of ice and the particle sizes encountered are such as to cause strong

variation in the albedo for single scattering. The size distributions containing many large particles were found to have a larger albedo for single scattering near 500 cm^{-1} than distributions with relatively few large particles. Therefore, the particle size can be estimated by choosing that distribution which produces the best fit between measured and calculated spectra, especially near 500 cm^{-1} .

Since variation of the size distribution and variation of the visible optical thickness do not produce mutually independent results, it is necessary to match the measured and calculated spectra while varying both parameters. The best fit between the measured and calculated spectra was found for the mean radius $\langle r \rangle$ equal to 2.0 μm and the visible optical depth equal to 0.4. The particle size distribution which produced the best fit to the measured spectrum was the cloud C.3 distribution of Deirmendjian (12). This particle size distribution falls to one-tenth of its maximum value at particle radii of 1.2 and 2.8 μm . The mode radius for the C.3 distribution is 2.0 μm , and thus the distribution is essentially symmetric about the mode radius. From the best-fit visible optical thickness the integrated

mass of the cloud was found to be $5 \times 10^{-5} \text{ g cm}^{-2}$. The integrated cloud mass inferred is necessarily an average over the field of view, and thus the actual integrated mass in the brightest regions of Fig. 2 may be $2 \times 10^{-4} \text{ g cm}^{-2}$ or slightly larger. This value can be contrasted with the integrated amount of H_2O vapor ($5 \times 10^{-3} \text{ g cm}^{-2}$) found in the nearby lower Arcadia spectrum. The source of the water forming the observed clouds is unknown. However, in view of the small amounts of H_2O vapor needed to form the cloud, surface outgassing is not required. Discussion of the evidence supporting either local degassing from the surface or orographic uplift coupled with convection has been presented by Leovy *et al.* (5).

Many spectra collected by the Mariner 9 IRIS contain spectral features indicative of H_2O ice. However, we have chosen the Tharsis Ridge spectrum for investigation because of its historical significance and because its strong thermal contrast favors quantitative interpretation of the ice features.

ROBERT J. CURRAN
BARNEY J. CONRATH
RUDOLF A. HANEL

VIRGIL G. KUNDE, JOHN C. PEARL
Goddard Space Flight Center,
National Aeronautics and Space
Administration, Greenbelt, Maryland

References and Notes

- G. de Vaucouleurs, *Physics of the Planet Mars* (Faber & Faber, London, 1961), pp. 77-98.
- S. A. Smith and B. A. Smith, *Icarus* **16**, 509 (1972).
- E. C. Slipher, *The Photographic Story of Mars* (Sky Publishing, Cambridge, Mass., 1962), pp. 27-36.
- C. B. Leovy, *J. Geophys. Res.* **76**, 297 (1971).
- , G. A. Briggs, B. A. Smith, *ibid.*, in press.
- See, for example, A. Dollfus, *Ann. Astrophys. Suppl.* **4** (1957), p. 114.
- R. A. Hanel, B. J. Conrath, W. A. Hovis, V. G. Kunde, P. D. Lowman, J. C. Pearl, C. Prabhakara, B. Schlachman, G. V. Levin, *Science* **175**, 305 (1972); R. A. Hanel *et al.*, *Icarus* **17**, 423 (1972); B. J. Conrath, R. J. Curran, R. A. Hanel, V. G. Kunde, W. C. Maguire, J. C. Pearl, J. A. Pirraglia, J. E. Welker, T. Burke, *J. Geophys. Res.* **78**, 4267 (1973).
- B. M. Herman and S. R. Browning, *J. Atmos. Sci.* **22**, 559 (1965).
- J. E. Bertie, H. J. Labb, E. Whalley, *J. Chem. Phys.* **50**, 4501 (1969).
- J. W. Schaaf and D. Williams, *J. Opt. Soc. Amer.*, in press.
- C. W. Hord, C. A. Barth, A. I. Stewart, A. L. Lane, *Icarus* **17**, 443 (1972); K. R. Blasius, *J. Geophys. Res.* **78**, 4411 (1973); A. J. Kilore, G. Fjeldbo, B. L. Seidel, M. J. Sykes, P. M. Woiceshyn, *ibid.*, p. 4331; S. S. C. Wu, F. J. Schafer, G. M. Nakata, R. Jordan, K. R. Blasius, *ibid.*, p. 4405.
- D. Deirmendjian, *Electromagnetic Scattering on Spherical Polydispersions* (American Elsevier, New York, 1969), pp. 77-83.

1 June 1973; revised 3 August 1973